Computed oscillations of a Confined Submerged Liquid Jet

Brett M. Gebert, Malcolm R. Davidson

G.K. Williams Cooperative Research Centre for Extractive Metallurgy
Department of Chemical Engineering, The University of Melbourne
Parkville, Vic. 3052, Australia

Murray J. Rudman

CSIRO, Division of Building Construction and Engineering, Highett, Vic 3190, Australia.

ABSTRACT

The jet oscillation observed in thin slab continuous casting is studied numerically by modelling the flow of liquid injected through a submerged entry nozzle and into a cavity. The oscillation relies on the exchange of fluid between recirculation cells on each side of the jet via a cross-flow through the gap between the nozzle shaft and the broad face of the cavity wall. Features of the oscillating jet are investigated by varying the resistance to cross-flow. This resistance occurs naturally since the nozzle obstructs cross-flow. The predicted oscillation can be manipulated by altering the cross-flow (through the use of an effective resistance force in the model) or stopped altogether to form a static asymmetrical flow pattern. Flow calculations are performed using a transient, two-dimensional, turbulent, fluid flow model.

1. INTRODUCTION

A large proportion of steel production involves the process of continuous casting. Ideally, the efficiency of this process can be maximised by casting at the thickness of the desired final product, thereby greatly reducing the energy requirements of the overall process. (For example, this would reduce the amount of hot rolling required.) However, to produce thin steel at the same volumetric rate as thick steel, the casting speed, and hence the inlet liquid jet velocity, must be faster and is inversely proportional to the slab thickness. The increased liquid jet velocity in *thin slab* casting (0.2 metres thickness or less) promotes an instability in the jet which oscillates by swinging from side to side across the broad face of the mould. For casting speeds greater than about 3m/min, this jet oscillation limits the quality of the product and the attainable thinness of the cast mould. Typically, these oscillations manifest themselves as surface waves and vortices. These in turn disturb the meniscus causing poor cast surface finish; they also entrain flux, resulting in lower bulk metal quality. The efficiency and quality of thin slab continuous casting could ultimately be improved by quantifying and understanding the oscillating flow. This would be achieved through improved control of the process.

In conventional continuous slab casting, the mould is thicker, velocities are lower, and a steady flow model is appropriate. Research into such casting has included metal delivery into the cast mould, cast strand behaviour and cast mould phenomena. Austin (1992) gives an overview of such research. Modelling of the fluid flow, including meniscus and surface effects, has been studied by various researchers for steady systems. For example, O'Connor and Dantzig (1994) developed a steady state 3D numerical model that computes the thermomechanical state in the mould; Najjar *et al.* (1995) investigated bifurcated nozzle design by predicting cast fluid flow using both 2D and 3D steady state numerical models; and Pericleous *et al.* (1995) investigated free surface flow and heat transfer in the casting process.

The bulk of existing published research on *thin slab* casting involves experimental simulations using a water model with no published theoretical model which includes

oscillatory flow and cross-flow past a submerged entry nozzle (SEN). Experimental water models have been used to simulate an oscillating jet, particularly with a bi-nozzle configuration (Gupta and Lahiri, 1994; Honeyands, 1994). A submerged jet injected into a blind cavity has been previously numerically modelled (Honeyands, 1994).

In casting moulds, fluid exits at the bottom of the geometry. Cross-flow through the gap between the nozzle shaft and the cavity wall is observed to be necessary for the oscillation to occur (Honeyands, 1994). When there is no gap the jet sticks to one wall. Cross-flow provides a coupling between the fluid on either side of the jet. Consequently, the pressure in the recirculation cell increases and drives the jet back past the cavity centreline. The cycle continues indefinitely and a sustained oscillation results.

The objective of the present study is to investigate numerically the regular cyclic behaviour of the oscillation and its dependence on the resistance to cross-flow. Physically, this resistance increases as the gap between the nozzle shaft and the cavity wall decreases. This work forms part of a larger research program aimed at a better understanding of the mechanisms of jet oscillation. The commercial computer flow solver CFX F3D (AEA Technology, 1995) is used to develop a two dimensional, single phase, transient, numerical model of the flow in the mould cavity.

2. MODEL FORMULATION

A two-dimensional rectangular flow geometry is chosen (Figure 1) because the mould thickness is much less than the width. An extension to three dimensions is deferred to a later study. A similar water model was developed by Honeyands (1994); however the Honeyands experiment is not simulated in this study because of difficulties representing the bottom outflow condition. There are no published results on a single jet nozzle in a geometry with free bottom outflow conditions. Honeyands (1994) numerically simulated the flow in a water model of a blind cavity and obtained predictions consistent with the experiments of Molloy (1972). That simulation has been confirmed in the present study. The depth/width ratio (= 4.8) of the geometry is chosen so that the predicted flow is independent of the depth.

Isothermal liquid flow is considered; the extension to include heat transfer and solidification in this oscillating system will be the subject of future work. Turbulence is represented using the standard $k-\epsilon$ model. This turbulence model has been used in other (non-oscillatory) studies of the casting process (e.g. Flint *et al.*, 1992; Najjar *et al.*, 1995).

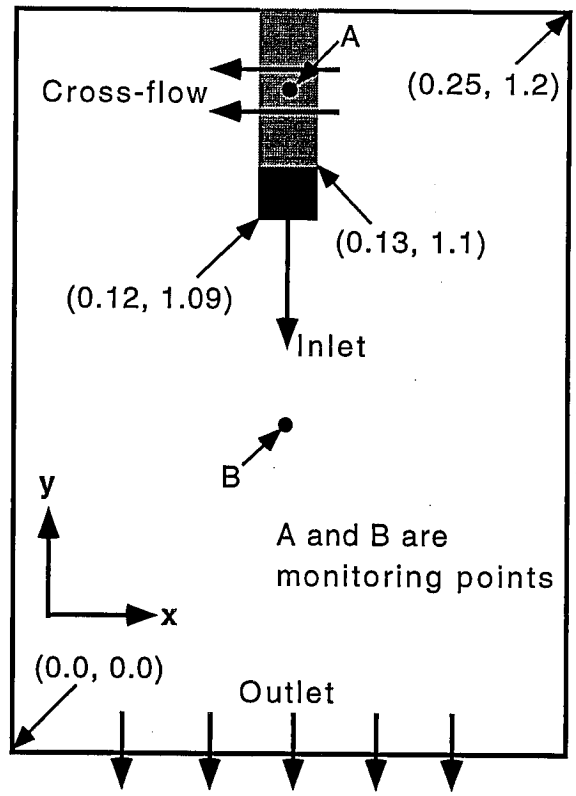

Figure 1: Schematic of flow geometry (not to scale). Co-ordinates shown are in meters. The black square defines the inlet whilst the gray area represents that region of the SEN across which a resistance to cross-flow is set. The velocity at each time step is recorded at monitoring points A and B.

To allow for cross-flow past the region occupied by the nozzle pipe in a two-dimensional model, the inlet flow must be represented as an internal mass source. This is achieved by defining the inlet as the lower

face of a small square region near the nozzle tip (the black square in Figure 1) which is removed from the flow domain. The top and side faces of this square region are taken to be no slip boundaries. A velocity profile consistent with the $\frac{1}{7}$th power law for fully developed turbulent pipe flow is assigned at the inlet. The average velocity is 2.0 m/s which translates to an effective casting rate of 0.08 m/s.

Resistance to cross-flow arises in practice from blockage caused by the SEN. To approximate this in a two-dimensional model, a resisting force of the form

$$K|v|v$$

is included in the momentum equation. K is a constant with units kg/m^4. A non-zero value is assigned to K in the region of the SEN (shown as the grey area in Figure 1). Resistance to cross-flow is related to the gap between the SEN and the broad face of the mould, and hence K should be a monotonic increasing function of SEN thickness. The form of this relationship depends on the geometry of the SEN cross-section and the gap thickness. Varying the coefficient K in the 2D model corresponds to varying the thickness of the SEN. The resisting force is chosen to be a function of v^2 because the pressure drop in contracting flows generally follow this relationship (Perry, 1984).

In practice, the top of the flow domain is a free-surface. This circumstance is approximated here by assigning a free-slip condition to the top horizontal boundary. No-slip boundary conditions together with wall functions are applied at solid walls. Zero normal gradient conditions are assigned to the outlet which includes the entire bottom boundary.

3. NUMERICAL CONSIDERATIONS

Solution of the flow equations is based on the SIMPLEC algorithm (Van Doormaal and Raithby, 1984) for the pressure-correction. All advected variables (except k and ϵ) are calculated using the third-order QUICK scheme. Although computationally expensive, this scheme was chosen since it provides minimal numerical diffusion, allowing the use of a reasonably coarse computational mesh.

The van Leer advection scheme was implemented for k and ϵ. This scheme is second order accurate and maintains monotonicity across computational cells hence preventing numerical oscillations in the solution domain. Other comparitive, higher order schemes became unbounded due to spurious oscillations. These, in turn, can induce negative values of k which results in indeterminate results.

The computational mesh and geometry of the model are both rectangular. Mesh density is non uniform and is concentrated in regions around the nozzle. The total number of mesh cells is 83 and 35 in the vertical and horizontal directions respectively.

An adaptive time-stepping algorithm was implemented to help reduce computation time. The average time step was around 9 ms. Time-step independence was confirmed by comparing results from the base case ($K = 100,000\,\mathrm{kg/m^4}$) with corresponding results using an average time step reduced by one third in both directions. The largest discrepency found for the predicted velocities at monitoring points was less than 5%.

Increasing mesh density by one third and comparing to the base case confirmed approximate mesh independence of the model. The largest difference found for the predicted velocities at the monitoring points was less than 10%.

The differences found in predicted velocities at the monitoring points were negligible when geometries with aspect ratios 4.8 and 6.0 were compared. Therefore the results can be considered independent of depth at an aspect ratio of 4.8.

4. RESULTS AND DISCUSSION

The four snap-shots in Figure 2 show predicted flow fields at *maximum jet deflection* (i.e. jet amplitude) for various values of cross-flow resistance K. A measure of jet

amplitude is the index I, defined as

$$I = 3 - \frac{(J-S)}{\frac{1}{2}W}. \qquad (1)$$

where S is the y-coordinate for the stagnation point of the impinging jet on the side wall at maximum jet deflection, J is the y-coordinate of the inlet and W is the width of the cavity. The index I increases as the jet amplitude increases. The number 3 in Equation 1 is arbitarily chosen so that the lowest value of I found in this study lies between 0 and 1.

In Figure 2(a), K is zero and the jet amplitude I is the largest for any K. Figure 2(b) shows a reduced value for I corresponding to an intermediate value of K ($200,000\,\mathrm{kg/m^4}$). In Figure 2(c) the smallest amplitude of the jet oscillation is achieved. This corresponds to the maximum value of K ($390,000\,\mathrm{kg/m^4}$) capable of producing an oscillation. All higher values of K prevent jet oscillation and a steady state, asymmetric flow field forms in which the jet sticks to one of the side walls. However as K increases above $390,000\,\mathrm{kg/m^4}$, the steady jet deflection also increases, reaching a maximum value asymptotically at infinite resistance. (Figure 2d).

The period of oscillation is plotted against K in Figure 3. For unhindered cross-flow ($K = 0$) the period is a minimum (6 seconds). The period then increases with K until a maximum value of around 10 seconds is attained at $K = 200,000\,\mathrm{kg/m^4}$. Then after a slight hump, the period remains fairly constant for $K > 200,000\,\mathrm{kg/m^4}$. For $K > 390,000\,\mathrm{kg/m^4}$ the oscillations cease. This value of K corresponds to a SEN thickness of approx. 75% of the cast thickness, based on a nozzle of circular cross-section.

The index of jet amplitude I is plotted against K in Figure 3. The maximum value of I occurs for unhindered cross-flow ($K = 0$). As K increases, I decreases linearly until a value of K is reached where oscillations are about to cease ($K = 390,000\,\mathrm{kg/m^4}$). This point coincides with the minimum value of I. As K increases further, steady jet deflection occurs, the magnitude of which increases with K until a maximum value of I is reached at infinite K.

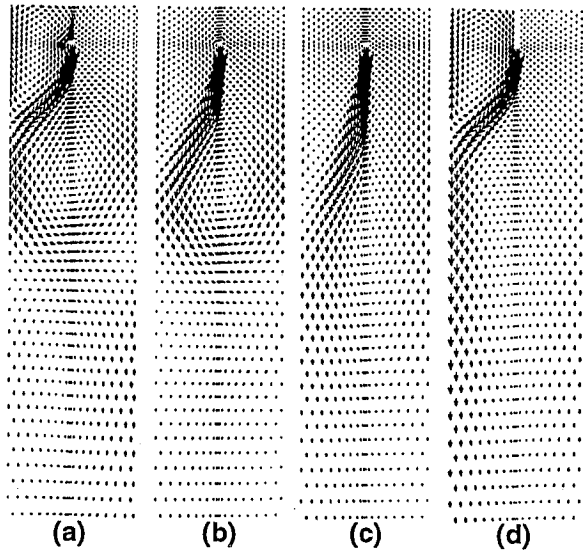

Figure 2: Velocity vector plots for varying cross-flow resistances at maximum jet deflection. The resistance values are as follows: (a)$K = 0$. (b)$K = 200,000\,\mathrm{kg/m^4}$ (intermediate). (c)$K = 390,000\,\mathrm{kg/m^4}$ (maximum for an oscillation to occur). (d)K = infinite (no cross-flow). (Note that the bottom 20% (approx.) of the geometry is omitted and that only every second mesh point is represented.)

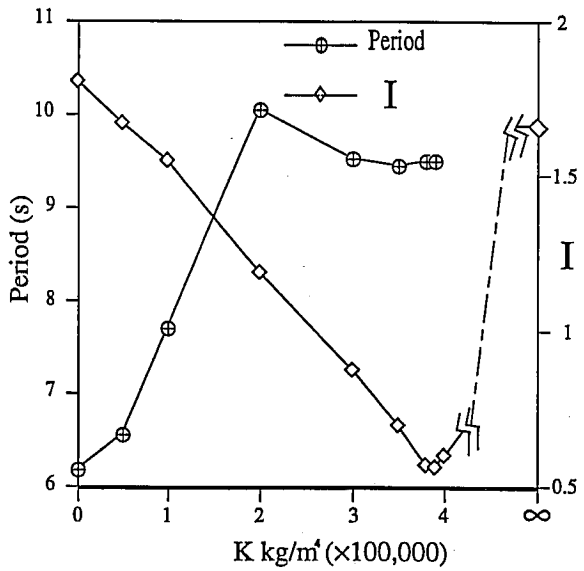

Figure 3: Period of oscillation and index of jet amplitude I vs. coefficient of resisting force, K.

Figures 4, 5 and 6 are all constructed

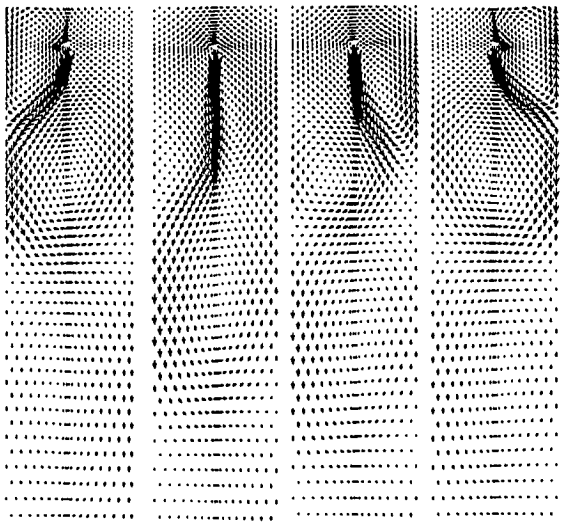

Figure 4: A sequence of four velocity vector snap-shots shown over half a period. These correspond to the schematics in Figure 6 and the graph in Figure 5. This cycle is for $K = 0$.

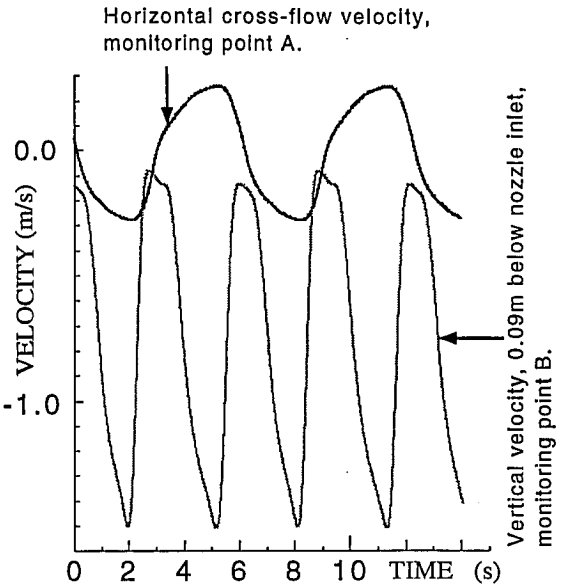

Figure 5: Velocities of the two monitoring points A and B vs. time for zero cross-flow resistance $K = 0\,\mathrm{kg/m^4}$. (Location of monitoring points are shown in Figure 1.) $t = 0$ coincides with maximum jet deflection (Figures 4(a) and 6(a)).

from the case where $K = 0$. Figure 4 shows four velocity vector snapshots taken over half a period (about $3.1s$). Of primary importance are the recirculation cells on either side of and below the jet, the direction of cross-flow, and the stagnation points on the side walls formed by the impinging jet. These features are illustrated as schematics in Figure 6. The predicted velocities at the monitoring points, A and B, are graphed against time in Figure 5.

Figure 4(a) corresponds to $t = 0$ in Figure 5 and shows the flow field at maximum jet deflection coinciding with negligible cross-flow velocity at the monitoring point A. Figure 4(b) corresponds to $t \approx 2s$ and is the time at which the maximum vertical velocity at the monitoring point B below the inlet region is found. Cross-flow from left to right (monitoring point A) is high but is still increasing in magnitude. Figure 4(c) represents the flow shortly after maximum cross-flow, $t \approx 2.3s$. The jet is now impinging on the opposite wall whilst cross-flow is rapidly declining. Figure 4(d) occurs at $t \approx 3.1s$ and is the mirror image of events at $t = 0$, i.e. one half cycle later.

In Figure 5, the vertical velocity at the monitoring points shows that a consistent cyclic jet oscillation has been achieved. Note that the oscillations at monitoring point B are not perfectly symmetrical. Two possible explanations have been considered: the computational sweep direction of the flow solver could provide a bias; or the transient results are inherently asymmetric despite symmetry in the geometry and boundary conditions. This issue has not yet been resolved.

Figure 6 is a schematic corresponding to the velocity vector snap-shots from Figure 4. Relative low pressure recirculation zones are shown as circles. A pressure difference between cells is indicated by **boldface** type, for the higher pressure cells, and standard type for the lowest pressure cell.

At maximum deflection (Figure 6a) there is negligible cross-flow occuring. Cell B is contracting and increasing in pressure. Cross-flow supplied from cell **A** begins to feed cell B due to the pressure differential which is 200Pa and decreasing. Conservation of mass in the region of cell B causes the jet to move back towards the centreline. Cell **A** is pushed towards the outlet region

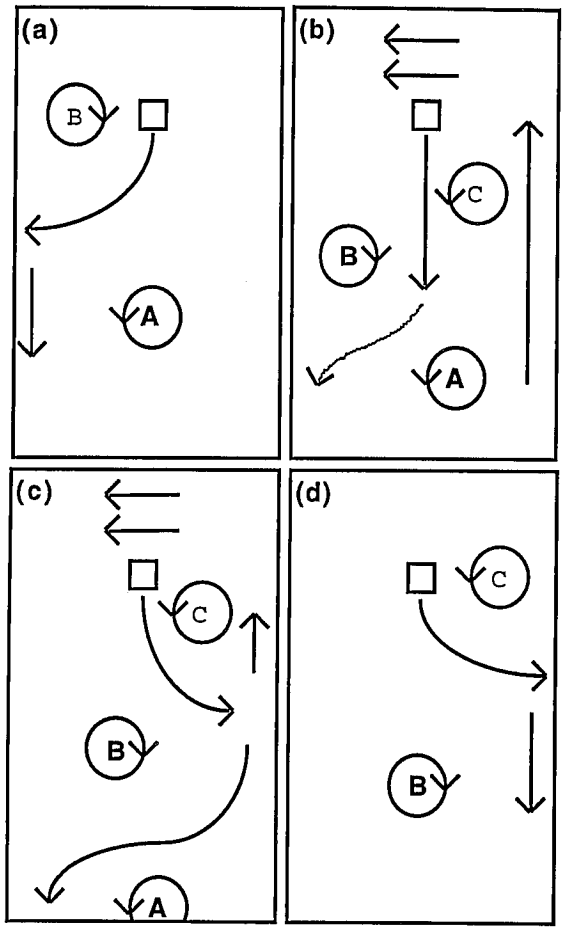

Figure 6: A sequence of schematics of the flow features over half a period. Plots (a)-(d) in this figure correspond to those in Figure 4. Regions A, B and C represent recirculation cells that approximately correspond to low pressure regions.

by the jet.

In Figure 6(b) the jet is approximately flowing through the centreline. Cell C has recently formed and is growing. The pressure difference between cell C and cells **A** and **B** is around 50 Pa. This differential pressure allows the jet to continue swinging towards the right wall. Cross-flow continues to increase from right to left and is being fed from recirculation cells **A** and C. Notice the flow running up the right wall from both cells **A** and C and that the jet contributes to this flow (Figure 4c). Cell **A** continues moving downwards.

In Figure 4(c), the pressure differential between cell C and cell **B** is 250Pa. The jet is now impinging on the right hand wall, forming a stagnant zone on the wall where the flow from the jet is split. This impingment eliminates the contribution of cell **A** on the cross-flow which begins to decline. The jet continues to deflect as the cross-flow diminishes to zero. Cell **B** moves down toward the outlet.

Figure 6(d), is the mirror image of Figure 6(a). Cross-flow reverses direction to counter the pressure differential (around 200Pa) between cell C and cell **B**. Cell C is contracting and increasing in pressure. The jet is at maximum deflection and soon cell **B** will disappear as did cell **A** and a new cell on the left hand side will form along the jet. The cycle continues indefinitely.

5. CONCLUSION

The important findings are summarised as follows:

- Increasing resistance to cross-flow reduces the magnitude of jet oscillation.
- Jet oscillations cease at a particular value of resistance to cross-flow.
- When oscillations are stopped by a high resistance to cross-flow, a static asymmetric flow field with a permanently deflected jet is produced.
- For the value of cross-flow resistance at which oscillations just cease, maximum jet deflection is a minimum.
- The period of jet oscillation increases with resistance to cross-flow, up to an intermediate value. For higher values of resistance the period is fairly constant. At the point where oscillations cease the period appears to jump from this constant value to infinity.
- Recirculation cells are formed by the oscillating jet. Flow between these recirculation cells is driven by pressure differentials and is connected via cross-flow

past the SEN and the broad face of the cavity wall.

6. ACKNOWLEDGEMENTS

This work was supported by the Australian Research Council and The University of Melbourne, using facilities provided by the G.K. Williams Cooperative Research Centre for Extractive Metallurgy, a joint venture between the CSIRO Division of Minerals and the Department of Chemical Engineering, The University of Melbourne.

7. REFERENCES

AEA Technology, (1995), *CFX F3D User Guide*, Release 4.1, AEA Technology, Harwell Laboratory, Oxfordshire, UK.

Austin, P.R. (1992) Literature survey on modelling of continuous casting. *BHP unrestricted Report*, report no. BHPR/PMR/R/92/044, Dec.

Flint, P.J., He, Q.L., Mahapatra, R.B. and Herbertson, J. (1992) Calibration of the fluid flow aspects of a continuous casting mould numerical model. *11th-AFMC'92, eds. M.R.Davis and G.J. Walker, Hobart*, Dec.

Gupta, D. and Lahiri, A.K. (1994) Water modelling study of the surface disturbances in continuous slab caster. *Metall. Mat. Trans. B.*, Vol.25B, p.227-233.

Honeyands, T.A. (1994) Flow dynamics in thin slab caster moulds. *PhD Thesis, University of Newcastle, Australia.*

Molloy, N.A., (1972), Oscillatory flow of a jet into a blind cavity II - experimental data, *University of Newcastle, NSW 2289, Australia*, EMR1/72.

Najjar, F.M., Thomas, B.G. and Hershey, D.E., (1995) Numerical study of steady turbulent flow through nozzles in continuous casting. *Metall. Mat. Trans. B*, Vol. 26B, Aug., pp.749-764.

O'Connor, T.B. and Dantzig J.A., (1994) Modelling the thin-slab continuous-casting mould. *Metall. Mat. Trans. B.*, Vol.25B, June, pp.443-447.

Pericleous, K.A., Chan, K.S. and Cross, M. (1995) Free surface flow and heat transfer in cavities. *Numerical Heat Transfer, Part B*, 27(4), pp. 487-507.

Perry, R.H. and Green, D. (1984) Perry's chemical engineer's handbook. *McGraw Hill*, 6th ed., pp.5-35.

Van Doormaal, J.P. and Raithby, G.D., (1984) Enhancements of the simple method for predicting incompressible fluid flows. *Numerical Heat Transfer*, Vol.7, pp.147-163.